Supporting Information

Synergistic Effect of Cu/Cu_2O Surface/Interface for Boosting Electrosynthesis of Ethylene from CO_2 in Zn-CO_2 battery

Zhichao Jia‡[a], Dandan Han‡[a], Fangfang Chang*[a], Xiaogang Fu[b], Zhengyu Bai*[a] and Lin Yang*[a]

a Collaborative Innovation Center of Henan Province for Green Manufacturing of Fine Chemicals, Key Laboratory of Green Chemical Media and Reactions, Ministry of Education, School of Chemistry and Chemical Engineering, Henan Normal University, Xinxiang, Henan 453007, P. R. China.

b State Key Laboratory of Solidification Processing, School of Materials Science and Engineering, Northwestern Polytechnical University, Xi'an 710072, P. R. China.

*Corresponding authors: changfangfang@htu.edu.cn (Fangfang Chang); baizhengyu@htu.edu.cn (Zhengyu Bai); yanglin@htu.edu.cn (Lin Yang)

EXPERIMENTAL SECTION

Chemicals. Copper (II) chloride dihydrate and sodium hydroxide were purchased from Tianjin Deen Chemical Reagent Co., Ltd. Sodium borohydride was obtained from China Piney Chemical Reagent Factory. Ethanol absolute was bought in Shanghai Wokai Biotechnology Co., Ltd. High purity CO_2 (Purity is greater than or equal to 99.999%) and N_2 were supplied by Beipu Special Gas Co., Ltd. All chemicals were analytical reagent grade and used without further purification.

Synthesis of catalysts

Synthesis of CuO nanosheets. CuO nanosheets were synthesized through a modified hydrothermal method .[1] In briefly, 0.341g $CuCl_2$ were dissolved in 20 mL deionized water and then mixed with sodium hydroxide solution (4.8 g NaOH). The solution was vigorously stirred for 25 min placed on a magnetic stirrer, and transferred to a 50 mL Teflon-lined autoclave. The Teflon-lined autoclave was sealed and maintained at 100 °C for 12 h, then allowed to cool to room temperature. The resulting copper oxide nanosheets were obtained by centrifugation with water and ethanol for four times. The product was finally dried in a vacuum oven at 60 °C for 4 h for further use.

Synthesis of 35% Cu/Cu_2O and 65% Cu/Cu_2O catalysts. In a typical preparation, 20 mg CuO nanosheets were dissolved in 20 mL deionized water to obtain solution A. The solution B was obtained by dissolving $NaBH_4$ in the deionized water and ethanol mixed solution (1:1, *V*/*V*). The solution B was injected into the solution A and stirred 1 h in an ice bath to obtain resulting products. The catalysts were obtained by tuning the molar ratio of solution A and B (A: B = 1:1 and 1:3). 35% Cu/Cu_2O was prepared when the molar ratio of solution A and B was 1:1 and 65% Cu/Cu_2O was prepared when the molar ratio of solution A and B was 1:3. The final products were obtained by centrifugation, washed with water four times, and dried in a vacuum oven at 60 °C.

Characterization. The morphology and microstructure of as-prepared catalysts were characterized by field emission scanning electron microscopy (FESEM) equipped with a Germany Zeiss SUPRA40 at an operating voltage of 15 kV and high resolution transmission electron microscopy (HR-TEM) equipped with JEOL-100CX at an operating voltage of 150 kV. X-ray photoelectron spectroscopy (XPS) measurements were performed on a PHI 5000C ESCA system. The pore structure was analyzed with N_2 adsorption-desorption measurements on a Brunauer-Emmett-Teller (BET) surface area analyzer (Quantachrome Instruments QuadraSorb SI4) and the pore size distribution was obtained by a Barrett-JoynerHalenda (BJH) model. X-ray powder diffractometer (XRD) was used to characterize the crystal structure of catalytic materials, performed on PANalytical Company with a scanning speed of 5°/min between 20° and 80°. The diffractometer was operated at 15～60 KV and 5～60 mA with Cu Kα radiation.

Electrochemical activity measurements. The catalyst ink was prepared by suspending 2.0 mg catalysts into 485 uL isopropanol and 15 uL Nafion solution (5 wt%), and then ultrasonicated for 30 min to form a homogenous ink.[2] 20 uL ink was drop-coated on the surface of the glass carbon disk (0.07 cm^2) and dried at room temperature. The electrochemical measurements were carried out in the electrochemical analyzer instrument (CHI760E) equipped with a gas-tight two-compartment H-cell separated by an ion exchange membrane (Nafion117), in which the glass carbon electrode coating catalysts, Ag/AgCl (saturated KCl solution) and platinum gauze were used as the working electrode, the reference electrode and counter electrode, respectively. 30 mL 0.5 M $KHCO_3$ solution was used as the electrochemical carbon dioxide electrolyte in cathodic and anodic cells. Prior to the experiment, the electrolyte was purged with N_2 or CO_2 for at least 30 min. Cyclic voltammetry curves (CV) were conducted to activate catalysts and then linear sweep voltammetry (LSV) curves was carried out in the potential range of 0.0 V to –1.4 V vs. RHE at a scan rate of 10 mV s^{-1}. In all measurements, the potential was converted to relative hydrogen electrode potential (RHE) using the following equation: $E_{\mathrm{RHE}} = E_{\mathrm{Ag/AgCl}} + 0.197 + 0.0591 \times \mathrm{pH}$. The electrochemical active surface area (ECSA) was derived from the capacitive current. The roughness of the catalysts was studied by cyclic voltammetry, which was performed in the electrolysis cell with CO_2 saturated 0.5 M $KHCO_3$. The scan rate of CV was from 40-120 mV s^{-1} with potential window from -0.05 to -0.15V (vs. RHE) and no reduction process occurred within this range. The geometric current density was plotted against the CV scanning rate. The double-layer capacitance was proportional to the roughness of the catalysts. The Zn-CO_2 battery tested in the H-type electrolytic cell was performed on the NEWARE battery tester. A polished zinc plate with an area of 2×0.5 cm^2 is used as the anode. The catalyst ink was prepared by dispersing 1 mg of 35% Cu/Cu_2O nanosheet catalyst in a mixed solution of 485 μL of isopropanol and 15 μL of 5 wt% Nafion. The catholyte is a mixture solution of 3 M $KHCO_3$ and 1.5 M KCl (pH 7.2). The electrode area of the cathode is 1.0×1.0 cm^{-2} (loading amount: 0.5 mg cm^{-2}). The anolyte is 6 M KOH and 0.2 M $Zn(CH_3COOH)_2 \cdot H_2O$ (PH value is 13.9). In the process of discharging, Zn is oxidized to Zn^{2+} at the anode, and CO_2 electro-reduction occurs at the cathode to generate electric energy; and during the charging process, Zn^{2+} on the positive electrode is reduced to Zn, and an oxygen evolution reaction occurs on the negative electrode.

Product analysis. Quantitative analysis of gaseous products (e.g., H_2, CO, CH_4 and C_2H_4) from the cathode chamber was performed using on-line gas chromatography (GC2030, SHIMADZU) equipped with flame ionization detector (FID) and thermal conductivity detector (TCD). The calibration curves were established using a series of standard gas mixtures (H_2, CO, CH_4, and C_2H_4 balanced in Ar, Yuanzheng). Gas product samples were measured more than three times every 30 minutes and standard errors were derived. The liquid products were collected 4 h after electrolysis and analyzed by ^1H NMR spectroscopy (Avance Neo, Bruker). The Faraday efficiency (FEs) was calculated by dividing the amount of charge transferred to each product by the total charge at a given time or throughout the reduction reaction (for liquid products). Each measurement was carried out three times to check the consistency with our experiment. The electrochemical data presented here were average values.

Density Functional Theory (DFT) Calculations. The DFT calculations were performed using the Cambridge Sequential Total Energy Package (CASTEP) code.[3, 4] The Perdew-Burke-Ernzerhof method with generalized gradient approximation of spin polarization was used to describe the exchange-correlation energy. The kinetic energy cutoff point of the plane wave basis group was set at 500 eV, and the Brillouin zone was integrated with k points of the 4 × 4 × 1 Monkhorst-Pack grid. A 15 Å vacuum space was constructed to avoid the interaction between adjacent slabs.

***In situ* attenuated total reflectance-surface enhanced infrared absorption**

spectroscopy (ATR-SEIRAS) Measurements. The ATR-SEIRAS measurements were examined in a two-compartment spectroelectrochemical cell comprising three electrodes including the working electrode, a platinum-wire as the counter electrode and a standard Ag/AgCl electrode as the reference. All the ATR-SEIRAS spectra were acquired using a Fourier Transform Infrared Spectrophotometer (FT-IR, Shimadzu.)

Turnover frequencies (TOFs) calculations.

TOF is defined as the frequency of reaction per active site, which is used to compare the intrinsic activity of each catalyst.[5] The TOFs of catalysts on GCEs in this study were calculated by the following equation:

$$TOF = \frac{j \times A}{4 \times \mathrm{F} \times n}$$

where *j* is according to the current density of the LSV curve, A is the geometric area, F is the Faraday constant, and n is the mole number of active sites on electrode that is calculated *via* the total loading mass from the following equation:

$$n = \frac{m_{loading}}{\mathrm{M}w} \times \gamma$$

where $m_{loading}$ is the loading mass of catalyst on GCE, $\mathrm{M}w$ is the molecular weight of catalyst and γ is the molar ratio of active atoms in the catalyst. In this work, the Cu atomic ratio of CuO, 35% Cu/Cu_2O and 65% Cu/Cu_2O catalysts is according to the results from XPS analysis. The TOF values of catalysts are listed at Table S3.

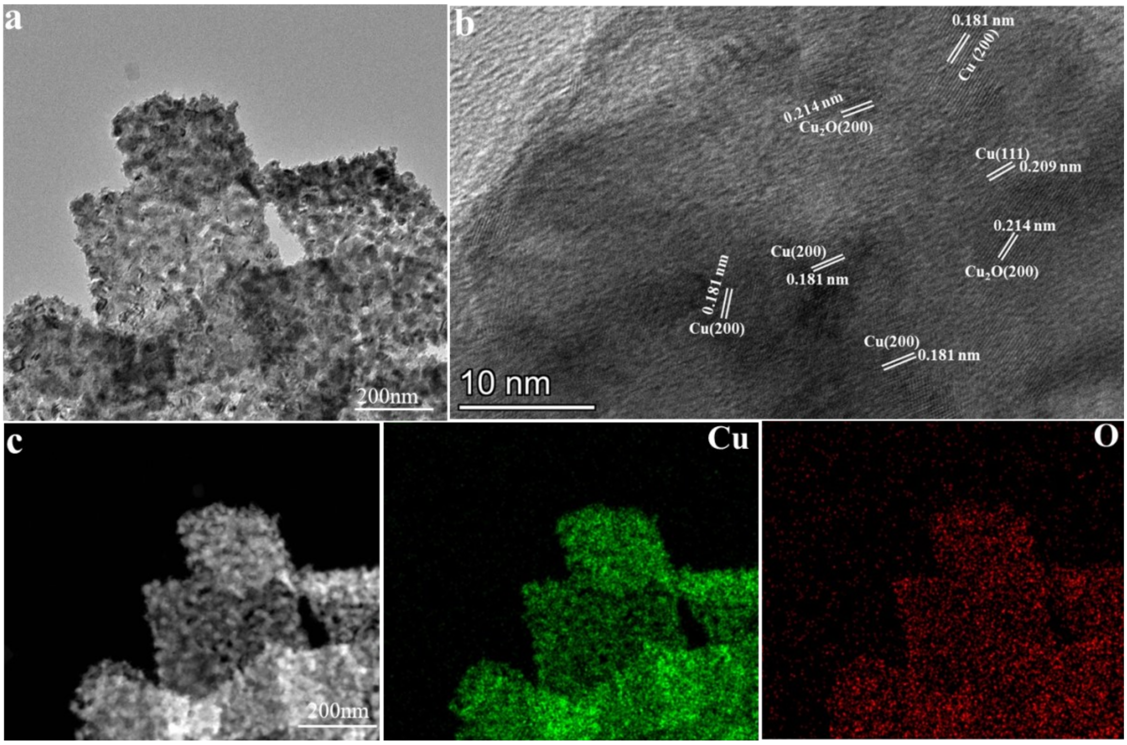

Fig. S1 TEM image (a) and HR-TEM image (b) and (c) elemental mapping of 65% Cu/Cu_2O

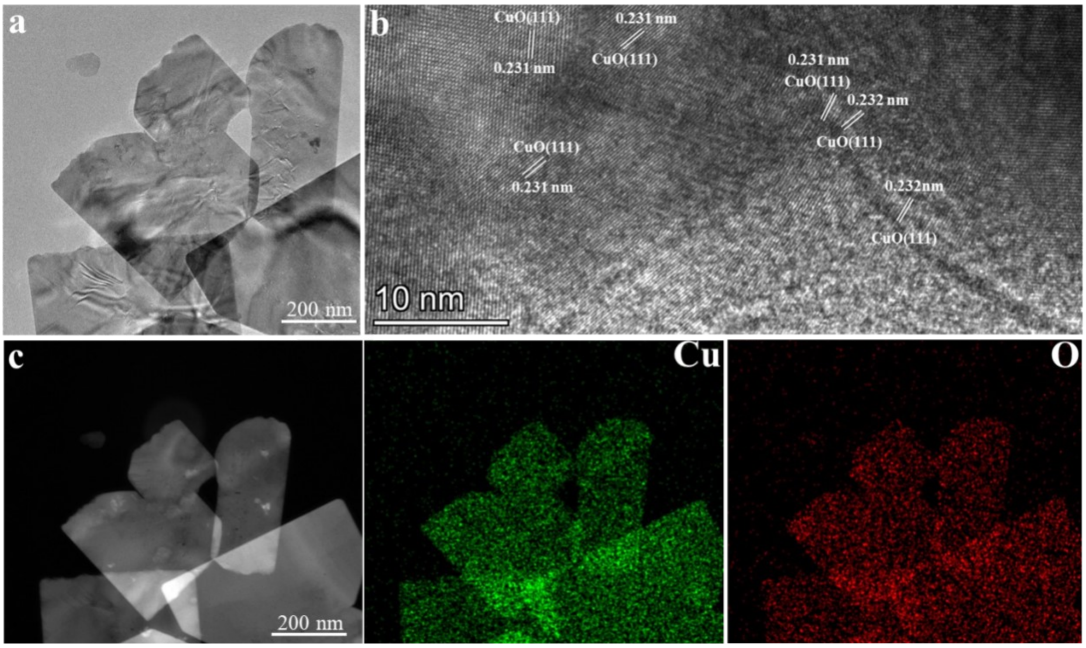

Fig. S2 TEM image (a) and HR-TEM image (b) of porous CuO, and (c) EDS-HAADF elemental mapping of porous CuO

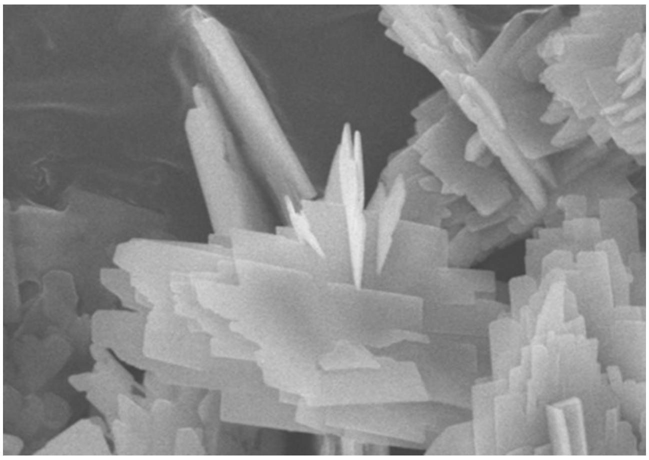

Fig. S3 SEM image of CuO nanosheets.

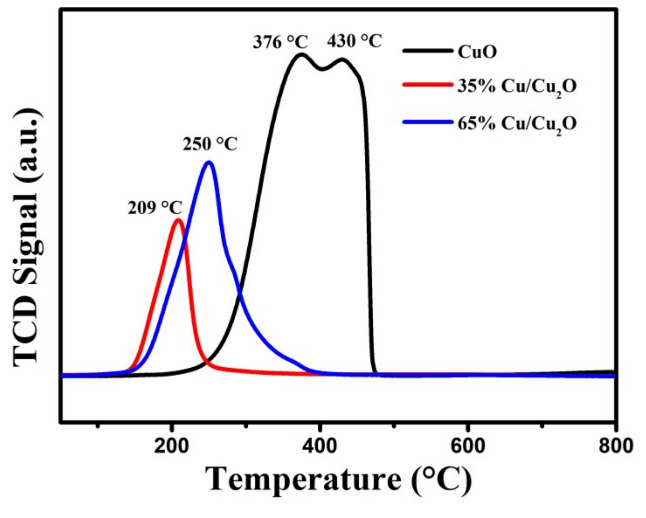

Fig. S4 H_2-TPR profiles of CuO, 35% Cu/Cu_2O, and 65% Cu/Cu_2O.

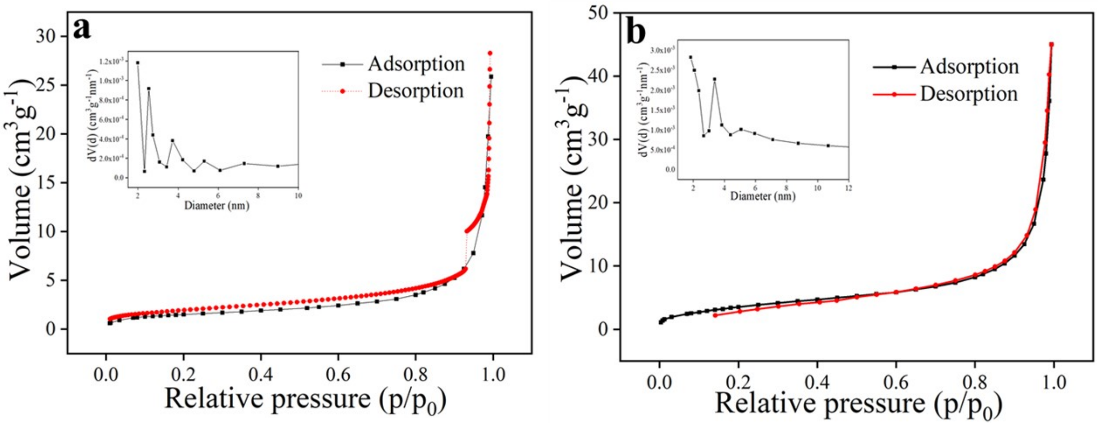

Fig. S5 N_2 adsorption-desorption isotherm of the 35% Cu/Cu_2O (a) and CuO (b). (Inset) Corresponding pore size distribution curve calculated from the desorption branch of the N_2 isotherm by the Barrett-Joyner-Halenda (BJH) formula.

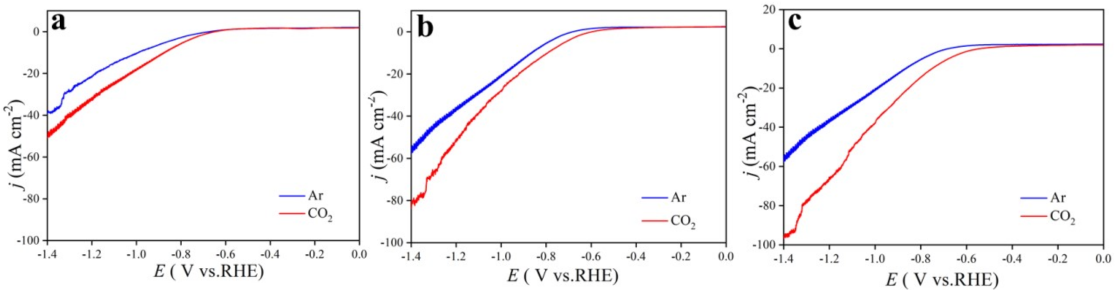

Fig. S6 LSV curves under Ar-and CO_2-saturated 0.5 M $KHCO_3$ of 65% Cu/Cu_2O (a), 35% Cu/Cu_2O (b) and CuO (c), scan rate: 10 mV s^{-1}.

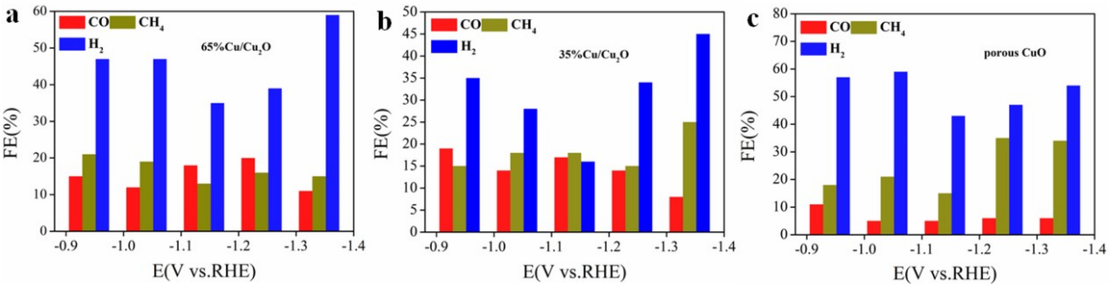

Fig. S7 FE for CO, CH_4 and H_2 over (a) 65% Cu/Cu_2O CuO, (b) 35% Cu/Cu_2O and (c) CuO electrodes at different applied potentials.

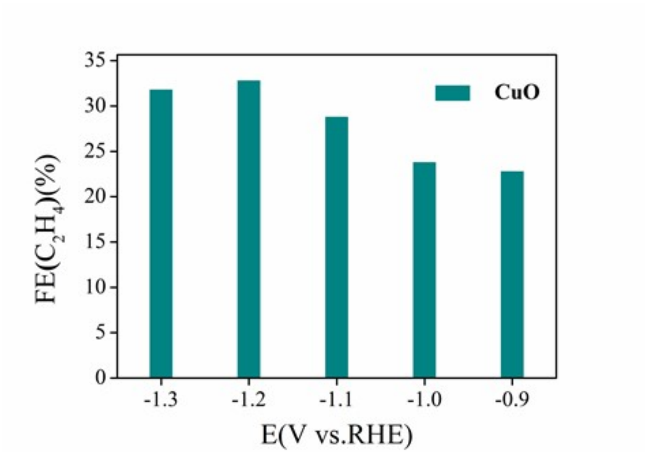

Fig. S8 FE for C_2H_4 over CuO electrode at different applied potentials.

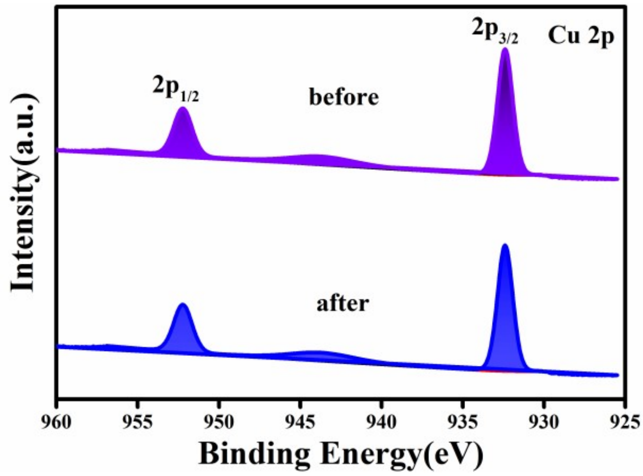

Fig. S9 The XPS before and after the I-t test for 35%Cu/Cu_2O.

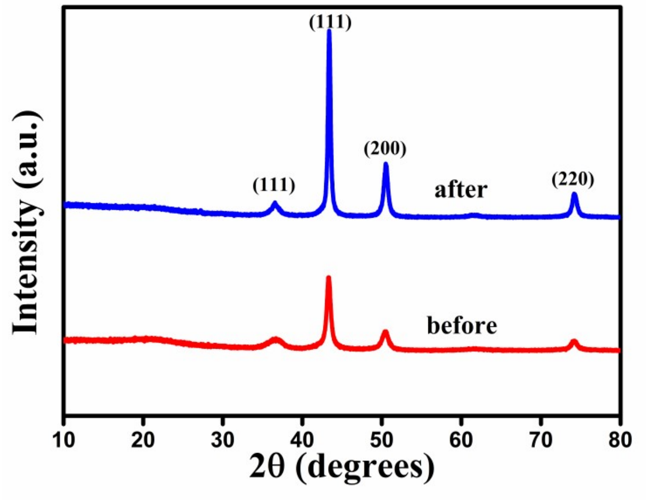

Fig. S10 The XRD before and after the I-t test for 35%Cu/Cu_2O.

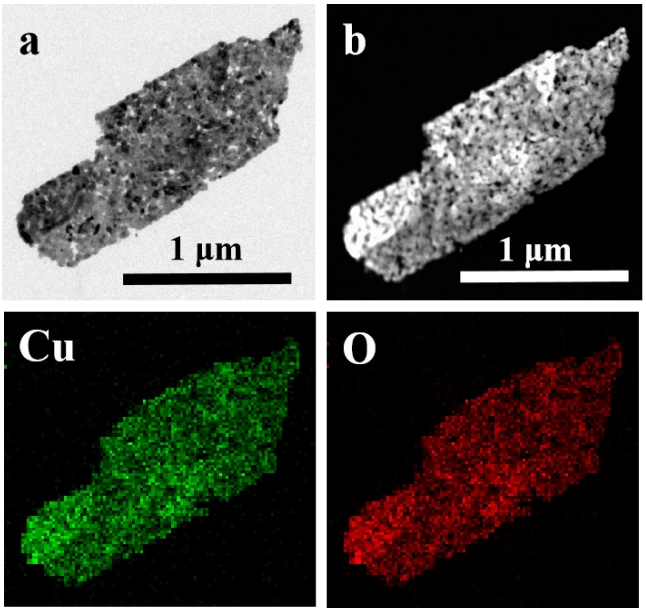

Fig. S11 The TEM after the I-t test for 35%Cu/Cu_2O.

Table S1. CO_2 reduction Faradaic efficiencies and current density of various catalysts in the potential range from -0.93 to -1.33 V (vs. RHE)

catalyst	**E (V vs. RHE)**	**j (mA cm^{-2})**	**Faradaic efficiencies for various products (%)**				**Total Faradaic efficiencies(%）**
			CH_4	CO	H_2	C_2H_4	_
65% Cu/Cu_2O	-0.9	7.5	15	21	47	16	99
	-1.0	14.2	12	19	51	18	100
	-1.1	27	18	13	35	34	100
	-1.2	35.5	20	16	39	26	101
	-1.3	36.8	11	15	59	14	99
35% Cu/Cu_2O	-0.9	14.5	19	15	35	30	99
	-1.0	18.5	14	18	28	40	100
	-1.1	35.8	17	18	16	50	101
	-1.2	43	14	15	34	37	100
	-1.3	57	8	25	45	22	100
CuO precursor	-0.9	13.8	5	15	55	23	98
	-1.0	21.2	11	32	33	24	100
	-1.1	26.9	9	11	49	29	98
	-1.2	35.4	5	6	56	33	100
	-1.3	45.3	3	8	54	32	97

Table S2. Comparison of Optimized C_2H_2 Products from Various Cu-Based Catalysts

Sample	**Electrolyte**	**E vs. RHE**	**Fradaic efficiency(%)** C_2H_4	**Ref.**
$AgCuO_x$	0.1 M $KHCO_3$	-1.1 V	42%	6
Oxygen-bearing copper	0.5 M $KHCO_3$	-0.95 V	45%	7
GMC-$[Cu_2(NTB)_2]$	0.1 m KCl	-1.278 V	42%	8
Oxygen-Cu (O-Cu)	0.1M $KHCO_3$	-1.08 V	38.1%	9
$Cu(OH)_2/Cu$	0.1 M $NaHCO_3$	-1.0 V	29%	10
$Cu@Cu_2O$	0.1 M $KHCO_3$	-1.2 V	35%	11
Cu_2O	0.1 M $KHCO_3$	-1.15 V	53%	12
35% Cu/Cu_2O	0.5 M $KHCO_3$	-1.10 V	50%	this work

REFERENCES

1. B. Zhang, J. Zhang, M. Hua, Q. Wan, Z. Su, X. Tan, L. Liu, F. Zhang, G. Chen and D. Tan, *J. Am. Chem. Soc.*, 2020, **142**, 13606-13613.
2. H. Jung, S. Y. Lee, C. W. Lee, M. K. Cho, D. H. Won, C. Kim, H.-S. Oh, B. K. Min and Y. J. Hwang, *J. Am. Chem. Soc.*, 2019, **141**, 4624-4633.
3. Q. Fan, C. Chai, Q. Wei, Q. Yang, P. Zhou, M. Xing and Y. Yang, *Mater. Sci. Semicond Process*, 2016, **43**, 187-195.

4. C. Nakib, A. Otmani, C. Djebbari, M. A. Amin, A. Djekoun, R. Boulechfar, H. Ferkous and Y. Benguerba, *J. Alloys Compd.*, 2022, **891**, 161950.
5. C. C. McCrory, S. Jung, J. C. Peters and T. F. Jaramillo, *J. Am. Chem. Soc.*, 2013, 135, 16977-16987.
6. J. Wang, Z. Li, C. Dong, Y. Feng, J. Yang, H. Liu and X. Du, *ACS Appl. Mater. Interfaces*, 2019, 11, 2763-2767.
7. W. Zhang, C. Huang, Q. Xiao, L. Yu, L. Shuai, P. An, J. Zhang, M. Qiu, Z. Ren and Y. Yu, *J. Am. Chem. Soc.*, 2020, 142, 11417-11427.
8. M. Balamurugan, H. Y. Jeong, V. S. K. Choutipalli, J. S. Hong, H. Seo, N. Saravanan, J. H. Jang, K. G. Lee, Y. H. Lee and S. W. Im, *Small*, 2020, 16, 2000955.
9. S. Y. Lee, H. Jung, N.-K. Kim, H.-S. Oh, B. K. Min and Y. J. Hwang, *J. Am. Chem. Soc.*, 2018, 140, 8681-8689.
10. G. Iijima, T. Inomata, H. Yamaguchi, M. Ito and H. Masuda, *ACS Catal.*, 2019, 9, 6305-6319.
11. L. Shang, X. Lv, H. Shen, Z. Shao and G. Zheng, *J. Colloid Interface Sci.* , 2019, 552, 426-431.
12. Y. Jiang, X. Wang, D. Duan, C. He, J. Ma, W. Zhang, H. Liu, R. Long, Z. Li and T. Kong, *Adv. Sci.*, 2022, 2105292.